Side chains affect the melt processing and stretchability of arabinoxylan biomass-based thermoplastic films

Chemosphere 294 (2022) 133618

Contents lists available at ScienceDirect

Chemosphere

journal homepage: www.elsevier.com/locate/chemosphere

Side chains affect the melt processing and stretchability of arabinoxylan biomass-based thermoplastic films

Parveen Kumar Deralia [a,*], Amit Kumar Sonker [a], Anja Lund [b], Anette Larsson [b], Anna Ström [b], Gunnar Westman [a,**]

[a] Chemistry and Biochemistry, Department of Chemistry and Chemical Engineering, Chalmers University of Technology, Kemivägen 10, SE-41296, Gothenburg, Sweden
[b] Applied Chemistry, Department of Chemistry and Chemical Engineering, Chalmers University of Technology, Kemivägen 10, SE-41296, Gothenburg, Sweden

HIGHLIGHTS

- Agri-waste biomass was valorized to produce stretchable thermoplastic films.
- ^{1}H NMR and FTIR confirmed the incorporation of butyl glycidyl ether.
- Melt processability in arabinoxylan was obtained with a low arabinose-to-xylan ratio.
- Larger side chains and a higher arabinose-to-xylan ratio increase elongation.

GRAPHICAL ABSTRACT

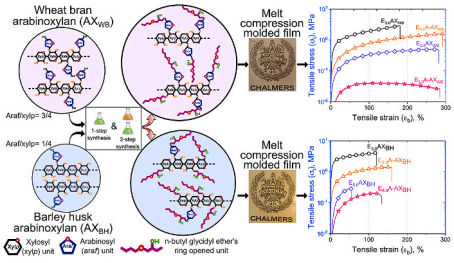

ARTICLE INFO

Handling Editor: Derek Muir

Keywords:
Biomass
Side-chain
Films
Melt processing
Themoplastic

ABSTRACT

Hydrophobization of hemicellulose causes melt processing and makes them stretchable thermoplastics. Understanding how native and/or appended side chains in various hemicelluloses after chemical modification affect melt processing and material properties can help in the development of products for film packaging and substrates for stretchable electronics applications. Herein, we describe a one-step and two-step strategy for the fabrication of flexible and stretchable thermoplastics prepared by compression molding of two structurally different arabinoxylans (AX). For one-step synthesis, the *n*-butyl glycidyl ether epoxide ring was opened to the hydroxyl group, resulting in the introduction of alkoxide side chains. The first step in the two-step synthesis was periodate oxidation. Because the melt processability for AXs having low arabinose to xylose ratio (araf/xylp<0.5) have been limited, two structurally distinct AXs extracted from wheat bran (AX_{WB}, araf/xylp = 3/4) and barley husk (AX_{BH}, araf/xylp = 1/4) were used to investigate the effect of araf/xylp and hydrophobization on the melt processability and properties of the final material. Melt compression processability was achieved in AX_{BH} derived samples. DSC and DMA confirmed that the thermoplastics derived from AX_{WB} and AX_{BH} had dual and single glass transition (T_g) characteristics, respectively, but the thermoplastics derived from AX_{BH} had lower stretchability (maximum 160%) compared to the AX_{WB} samples (maximum 300%). Higher araf/xylp values, and thus longer alkoxide side chains in AX_{WB}-derived thermoplastics, explain the stretchability differences.

* Corresponding author.
** Corresponding author.
E-mail addresses: deralia.parveen@gmail.com (P.K. Deralia), westman@chalmers.se (G. Westman).

https://doi.org/10.1016/j.chemosphere.2022.133618
Received 25 August 2021; Received in revised form 3 January 2022; Accepted 11 January 2022
Available online 20 January 2022

1. Introduction

The pursuit of a sustainable and biobased economy has resulted in the development of technologies for the conversion of polysaccharide-based polymers such as arabinoxylan to materials and chemicals. In this context, the use of industrial polymer processing techniques for thermoplastic materials, such as injection molding, compression molding, etc., is preferred due to the minimal solvent requirement, scalability, fast, and efficient processing (Martello et al., 2014). A recently developed synthesis method has demonstrated melt processability in arabinoxylans with a ratio of α-L-arabinofuranosyl units (araf) to β-(1, 4)-linked xylopyranosyl units (xylp) greater than 0.7 (Börjesson et al., 2019b; Deralia et al., 2021a, 2021b). Despite this progress, it is unclear whether arabinoxylans with low araf/xylp (<0.5), such as barley husk arabinoxylan and xylan, can be processed in a melt. The structural complexity of arabinoxylans, as well as their variation with their botanical origin and isolation methods, influence how we can process them for chemicals and materials. By studying such interactions, we can learn about polymer structures and their structure-property relationships, such as the correlation between polymer composition and stretchability. This will help broaden the potential application spectrum for the development of advanced materials and polymer science and will be critical to the development of enabling technologies for future biorefineries (Ibn Yaich et al., 2017). In this study, we isolated arabinoxylans from two major agricultural waste streams, wheat bran and barley husk, to obtain two structurally different arabinoxylans (high and low araf/xylp, respectively), and subjected them to two different chemical modification strategies with the goal of enabling melt processability and identifying structure and compositional factors.

Wheat and barley grains have external protective envelopes called husk and bran. Cereal/agrowaste products, such as wheat bran and barley husk, are valued for their renewability and abundance. These agricultural wastes are currently fed to livestock. These feedstocks require comprehensive and efficient valorization approaches to compete with and replace fossil-based products (Apprich et al., 2014). These are primarily composed of cellulose, arabinoxylan, lignin, and other carbohydrate polymers. Because of their excellent functionality, these natural polymers can be used as materials. Significant attention has been paid to the use of cellulose and lignin in the production of biobased chemicals and materials.

Xylan is the second most common polysaccharide polymer in plants after cellulose. Cereal arabinoxylan structures are much more complex and diverse than cellulose structures and differ between plants. For example, wheat bran arabinoxylan (AX_{WB}) has a higher ratio of α-L-arabinofuranosyl units (linked at positions C-2 and/or C-3) to main-chain β-(1,4)-linked xylopyranosyl subunits linked to the main chain (araf/xylp = 0.7 to 1.1) than barley husk arabinoxylan (AX_{BH}) (araf/xylp = 0.1 to 0.4) (Börjesson et al., 2018a, 2019b; Deralia et al., 2021a; Gebruers et al., 2008; Izydorczyk and Dexter, 2008; Köhnke et al., 2008; Ruthes et al., 2017; Schooneveld-Bergmans et al., 1999). Due to this distinction, intramolecular interactions loosen in AX_{WB}, resulting in greater flexibility in solution and, as a result, greater water solubility than in AX_{BH} (Pitkänen et al., 2009; Selig et al., 2015). Taking advantage of these inherent and diverse functionalities and properties, it is critical to design and synthesize more diverse functionalized materials based on AX with the goal of broadening the application spectrum.

AX's hydrophilicity and brittleness are two major barriers that prevent it from being used in thermal processing techniques such as melt-compressing molding, etc. It is an amorphous polymer with a dense hydrogen-bonded network that makes it brittle and melt non-processable. Strong hydrogen bonding appears as a narrow window between the melting/glass transition temperature (T_m or T_g) and the degradation temperature (T_d). For these reasons, AX must be chemically modified to further disrupt hydrogen bonding and reduce the T_g downshift from T_d. Chemical modifications (Ibn Yaich et al., 2017), such as esterification, etherification, oxidation are commonly used to improve the processability, properties (Mikkonen et al., 2015; Stepan et al., 2012) and functionality of hemicellulose such as thermoplasticity (Börjesson et al., 2019b; Jain et al., 2000), hydrophobicity (Fredon et al., 2002; Hartman et al., 2006; Nypelö et al., 2016; Peresin et al., 2012) and conductivity (Hansen and Plackett, 2008). Hemicelluloses, even after chemical modification, can be processed using only organic solvents. As a result of the high cost of solvents and the time-consuming nature of the process, scaling up via solvent processing is not feasible. It would be advantageous if hemicelluloses could be processed using industrial polymer processing methods such as melt extrusion and melt compression molding to harness their functionality in products. These processing methods allow for quick processing without the use of solvents and require little energy. To create thermoplastic xylans, the xylans were etherified by hydroxypropylation and *n*-butyl glycidyl ether (BuGE) (Jain et al., 2000; Laine et al., 2013). Melt processing of cellulose, cellulose acetate, and starch has been shown to be effective with and without the addition of external plasticizers (Averous and Pollet, 2014; Chen et al., 2018; Mathew and Dufresne, 2002; Zepnik et al., 2013). External plasticizers, when used, migrate and recrystallize over time, resulting in poor product performance and shorter shelf life of thermoplastic materials; additionally, they should be environmentally friendly. Melt processing of hemicelluloses has not previously been reported (Börjesson et al., 2019a, 2019b, 2019a).

An alkylketene dimer and an alkenyl succinic anhydride were used to hydrophobize xylan in a recent study, but thermoplasticity was not achieved (Cheng et al., 2021). Previous studies have demonstrated that ring opening polymerization of ε-caprolactone on hemicellulose can make it melt processable (Farhat et al., 2018; Svärd et al., 2018) We previously demonstrated that AX with a high araf/xylp (0.8 and 1.1) after one-step and two-step functionalization with BuGE can potentially be processed using the polymer processing technique (Börjesson et al., 2019a, 2019b; Deralia et al., 2021a, 2021b). In these studies, AX hydroxyl groups were deprotonated into alkoxides after reaction with epoxides. We also discovered a link between the molar substitution of BuGE and the properties of AX-derived thermoplastics.

Thermal processability, on the other hand, was only achieved when araf/xylp was between 0.8 and 1.1 (Börjesson et al., 2019a, 2019b; Deralia et al., 2021a, 2021b). It remains to be discovered how and why AX with a specific structure and composition enables thermal processing and produces flexible and stretchable thermoplastic materials. In this regard, AX with different araf-xylp can be obtained a) by enzymatically tailoring the araf-xylp and b) by selecting two naturally available polymers with different araf/xylp. The first is time consuming due to the scarcity of pure enzyme components capable of attaching specific sites (Sheldon and Brady, 2018). On the other hand, the latter has the advantage of being readily available and is a representative of true industrially feedstock-isolated polymers. Furthermore, the next challenge is to efficiently harness the significant untapped potential of the inherent structural complexity and diversity of AX polymers, from industrially available feedstocks to materials.

As a result, we set out to learn more about the structural composition and property attributes of AX in terms of melt processability. In this study, we used wheat bran and barley husk to extract arabinoxylans with varying araf/xylp ratios. The primary goal is to see if melt processability can be achieved in barley husk arabinoxylan (low araf/xylp). We create AX-derived thermoplastic materials with a wide range of flexibility and thermal properties by utilizing different araf/xylp of AXs and elongating existing groups and/or creating new alkoxide chains with BuGE. The melt compression molding technique is used to process the modified AX materials. We also attempted to establish a link between the chemical structure and stretchability.

2. Experimental

2.1. Reagents and materials

Wheat bran and barley husk were supplied by Lantmännen AB (Stockholm, Sweden) (dry matter 90%). Arabinoxylan (AX) was isolated from wheat bran and barley husk with minor changes according to previous literature (Börjesson et al., 2018a) and details are provided in the Supplementary Material. The carbohydrate compositions and relative molar masses of the extracted arabinoxylans are given in Tables S5 and S6. The purities of the extracted AXs from wheat bran and barley husk were 75 and 89.7%, with the rest consisting of salts, lignin and proteins and were used for etherification reactions without further purification. All chemicals, reagents, enzymes, and solvents were purchased from Sigma-Aldrich (Schnelldorf, Germany) or Fisher Scientific (Sweden), with the exception of ethanol, which was purchased from Solveco AB (Sweden). Unless otherwise noted, the chemicals were used exactly as supplied. Deionized water was used. Spectrum Laboratories Inc., CA, USA, supplied the dialysis tubing (Spectra/Por, MWCO 3500). Fig. 1a shows a simplified scheme of the experimental approaches used in the study.

2.2. Synthesis of arabinoxylan ether (E-AX) and activated arabinoxylan ether (E-A-AX)

Extracted AX was activated by a series of periodate oxidation and reduction steps, according to previous research (Fig. 1c) (Amer et al., 2016; Siller et al., 2015). Activated AX and extracted AX were etherified (Fig. 1b and c) according to the reported literature (Nypelö et al., 2016). The Supplementary Material contains information on the AX activation and synthesis of arabinoxylan ether and activated arabinoxylan ether. Table 1 summarizes the sample codes and the characterization and synthesis parameters used in the study.

2.3. Compression molding and preparation of samples

Compression molding and solution casting were used to fabricate films and the Supplementary Material contains more information. For tensile testing, rectangular specimens with gauge dimensions of 20 mm length, 5.6 mm width and 0.4 mm thickness (0.1 mm thickness for solution cast film) were cut. DMA was performed on rectangular specimens with dimensions of 30 mm in length, 6 mm in width and 0.4 mm in thickness (0.1 mm thickness for solution-cast films). The films were cut into rectangular shaped samples using a parallel razor-blade cutter.

2.4. Characterization

The level of oxidation was determined by measuring periodate consumption using UV–vis and reduction in sugar content using HPLC (Equations 1 and 2 in the Supplementary Material) after activation. The Supplementary Material contains more details on calculation of the oxidation level.

Samples were hydrolyzed in two stages with sulfuric acid according to the NREL procedure (Sluiter et al., 2010). A 1 ml aliquot of the hydrolyzed sample was used for carbohydrate analysis, and the remainder was neutralized, freeze dried, and then used for ^{1}H NMR analysis. HPLC and NMR were used to determine the substitution of *n*-butyl glycidyl ether (BuGE). Details on BuGE substitution are given in the Supplementary Material. Solubilized monosaccharides were quantified using a Dionex ICS-4000 HPAEC system equipped with PAD (both from Dionex, Sunnyvale, CA, USA) coupled to a Dionex CarboPac PA1 analytical column for carbohydrate analysis. ^{1}H NMR spectra of freeze-dried samples dissolved in 0.7 ml of NMR grade D_2O at 50 °C for 1 h were recorded on a Varian MR-400 MHz spectrometer (Agilent Technologies) at 25 °C. The Supplementary Material contains information on ATR-FTIR, GPC, DSC, TGA, DMA and Tensile testing.

3. Results and discussion

3.1. Synthesis of arabinoxylan ether (E-AX) and activated arabinoxylan ether (E-A-AX)

Using 3 and 5 mol of BuGE from wheat bran arabinoxylan (AX_{WB}) and barley husk arabinoxylan (AX_{BH}), a series of AX ethers and activated AX ethers were successfully synthesized (Fig. 1b and c; reaction parameters in Table 1). IR was used to confirm the BuGE substitution in the polymer. Peaks at 3000-2850 cm^{-1} (CH stretching), 1500-1350 cm^{-1} (CH bending), and 740 cm^{-1} (CH_2 rocking) (Coates, 2006; Wang and Somasundaran, 2006) confirm the formation of an ether link between the polymer hydroxyl group and the BuGE epoxide ring (Fig. 2a and b).

The peak at 3300 cm^{-1} (OH stretching) shifts slightly toward the high wavenumber, indicating that the hydrogen bonding in E-AX and E-A-AX is loosening. ^{1}H NMR provided qualitative confirmation of BuGE substitution. Because molar substitution increases with increased BuGE moles, molar substitution (MS) and intact carbohydrate substitution (ICS) data [MS-Equation 5 and ICS- Equation 3 in the Supplementary Material] support the successful introduction of BuGE into polymers (Fig. 2c and Table S6). A consistent observation is that the molar substitutions of E-A-AX are higher compared to E-AX, contrary to the results of a previous report (Börjesson et al., 2019b). This means that this oxidation level does not necessarily translate into an increase in MS when 3 and 5 mol of BuGE are used because the ring-opened sugar units upon oxidation may create a steric obstacle that causes OH groups to be hampered. However, IR and ^{1}H NMR determined MS results are consistent with previously reported findings (Börjesson et al., 2019a, 2019b; Deralia et al., 2021a, 2021b; Härdelin et al., 2020).

A sugar unit, with an alkoxide terminal after BuGE is attached to the hydroxyl group, is no longer a monosaccharide and will not be detected as a monosaccharide in carbohydrate analysis of etherified samples. We can calculate the BuGE substitutions in sugar units by measuring the carbohydrate content of the samples before and after etherification. Intact carbohydrate substitutions (ICS) refer to carbohydrate units (pentose and hexose) that have not been affected by the pre-activation step in two-step synthesis and have reacted with BuGE, as well as carbohydrate units that have reacted with BuGE in one-step synthesis (ICS).

Thus, ICS denotes the fraction of sugar units whose OH groups have been substituted with BuGE monomers and it quantifies only BuGE substitutions on sugar units (Equation 3 in the Supplementary Material). Similarly, intact xylose substitutions (IXS) and intact arabinose substitutions (IAS) [Equations 6 and 7 in the Supplementary Material] quantify BuGE substitutions alone xylose and arabinose units. Note that the ^{1}H NMR molar substitution (MS) values include all possible reaction sites, i.e., the hydroxyl groups of sugar units, the alkoxide moieties (BuGE epoxide ring-open structure) and ring-open sugar units after activation. Because intact arabinose substitutions (IAS) are greater than intact xylose substitutions (IXS), arabinosyl unit substitutions on the side chains are preferred over xylosyl unit substitutions in the polymer backbone (Table S5). In $E_{3.0}AX_{WB}$ and $E_{3.0}AX_{BH}$, for example, intact arabinose substitutions (IAS = 0.68 and IAS = 0.78) are greater than intact xylose substitutions (IXS = 0.51 and IXS = 0.69) (Table S5). When 3 mol of BuGE were used, the difference in BuGE substitutions in arabinosyl and xylosyl units was greater between the AX_{BH} and AX_{WB} ether samples than when 5 mol of BuGE were used (Table S5). These findings are attributed to a higher araf/xylp (3/4) in AX_{WB} (compared to a lower araf/xylp (1/4) in AX_{BH}) that sterically hinders BuGE substitution.

The relative molar masses determined by GPC are shown in Fig. 2d and Table S6. Figures S2-S5 show the molar mass distribution curves that have multimodal peaks. These multimodal peaks indicate the presence of multiple polymeric fractions in the samples (Figures S5-S7 and Table S7). There are more peaks in the AX_{WB} samples than in the AX_{BH} samples. Note that the purity of the extracted AX_{WB} and AX_{BH} are ≈75 and 90%, respectively, with the remainder consisting of salts, lignin, and proteins. The M_ws of the AX_{WB} and AX_{BH} ethers are lower

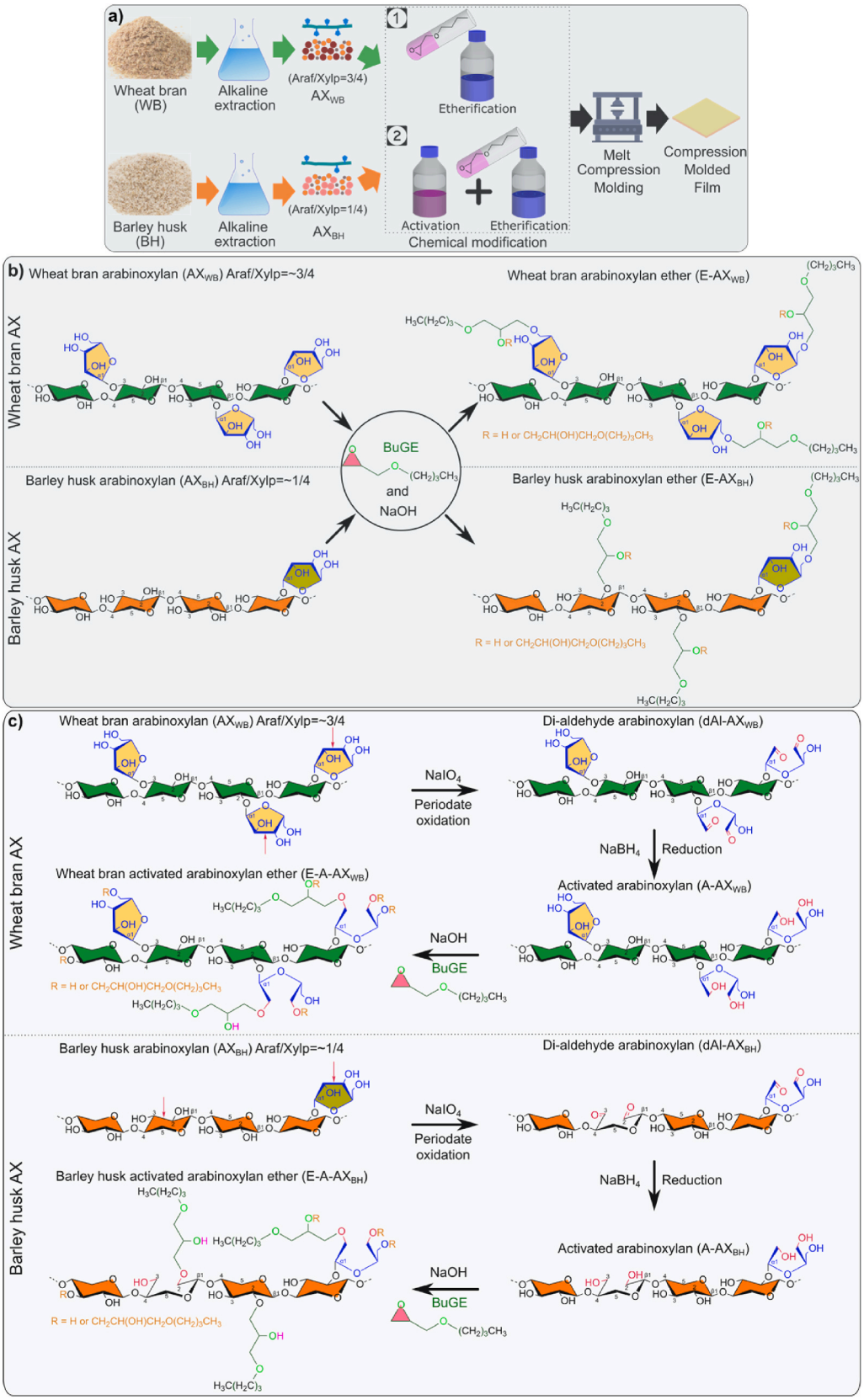

Fig. 1. a) Schematic diagram of the experimental steps. Araf/Xylp denotes the ratio of arabinosyl to xylosyl units in the extraction arabinoxylan (AX), and *n*-butyl glycidyl ether (BuGE) was used for hydrophobization. In this study, two chemical modification strategies were used: hydrophobization alone ① and hydrophobization with preactivation ②. Schematic presentation of the two synthesis procedures used to obtain thermoplastic AX. **b)** Arabinoxylans were directly etherified with *n*-butyl glycidyl ether (BuGE) to obtain AX ethers in the first synthesis procedure. **c)** Arabinoxylans were first activated by successive periodate oxidation and reduction and then etherified with BuGE to obtain activated AX ethers in the second synthesis procedure.

Table 1
Sample codes, synthesis parameters and characterization of arabinoxylan ether (E-AX) and activated arabinoxylan ether (E-A-AX).

Entry[a]	Sample ID[b]	PI/ASU[c], mole	Oxidation level 1[d], %	Oxidation level 2[e], %	NaOH and BuGE/ASU[f], mole
1	$E_{3.0}AX_{WB}$	–	–	–	3
2	$E_{5.0}AX_{WB}$	–	–	–	5
3	$E_{3.0}AX_{BH}$	–	–	–	3
4	$E_{5.0}AX_{BH}$	–	–	–	5
5	$E_{3.0}A\text{-}AX_{WB}$	0.25	19	24	3
6	$E_{5.0}A\text{-}AX_{WB}$	0.25	19	24	5
7	$E_{3.0}A\text{-}AX_{BH}$	0.25	15	28	3
8	$E_{5.0}A\text{-}AX_{BH}$	0.25	15	28	5

[a] Entry 1–4 and 5–8 are synthesized without and with activation, respectively.
[b] In E_xAX_y (entry 1–4) and $E_xA\text{-}AX_y$ (entry 5–8) x denotes the number of *n*-butyl glycidyl ether (BuGE) moles, y denotes the origin of AX (wheat bran or barley husk), and A stands for the activated AX.
[c] mole of periodate (PI) per anhydrous sugar unit (ASU) [includes pentose and hexose, sum of xylan, arabinan and glucan] and the reduction reaction parameters were similar for all reactions.
[d] Oxidation level determined from periodate consumption using UV–vis (see Equation 1 in Supplementary Material).
[e] Oxidation level based on the reduction of sugar content after activation (see Equation 2 in Supplementary Material).
[f] mole of NaOH and *n*-butyl glycidyl ether (BuGE) per anhydrous sugar unit (ASU).

than those of AX_{WB} and AX_{BH} (Table S6). The M_w of AX_{WB} is higher (46 kDa) than that of AX_{BH} (21 kDa). Furthermore, degradation as a result of the reaction's strong alkaline medium and precipitation with methanol used to recover the product could have caused this decrease in M_w. The decrease in M_w of E-A-AX_{WB} and E-A-AX_{BH} is even more pronounced as a result of the degradation that occurred during the activation step (successive periodate oxidation and reduction) and the precipitation step (Börjesson et al., 2018b; Saito et al., 2012). Because of the insolubility of these samples in DMSO/LiBr, M_ws of A-AX_{WB} and A-AX_{BH} could not be obtained. However, a decrease in molecular weights and a narrowing of the molecular weight distribution (MWD) are anticipated. This work provides indirect proof of these observations because both AX_{WB} and AX_{BH} derived samples have molecular weights lower than those of their starting materials, i.e., AX_{WB} and AX_{BH}. Furthermore, because the polydispersity indices are reduced, their molecular weight distributions (MWD)s are narrowed (Figures S2-S4, Fig. 2d and Table S6). Previous studies have also reported degradation after periodate oxidation, resulting in a decrease in M_w (Börjesson et al., 2018b; Muhammad et al., 2020) and polydispersity indices (Muhammad et al., 2020).

3.2. Melt compression molding

We used melt compression molding (at 140 °C under 50 kPa pressure for 3 min), one of the industrial polymer processing techniques, to determine the thermal processability of the synthesized samples. All synthesized samples were successfully compressed, and the resulting films are shown in Fig. 3b and c.

The films were foldable and flexible (Fig. 3d and e). Compression moldability of AX_{WB} synthesized samples with araf/xylp of 3/4 was expected (Fig. 1c) and has previously been demonstrated when the araf/xylp ratios were 0.8 and 1.1 (Börjesson et al., 2019a, 2019b; Deralia et al., 2021a). The AX_{BH} synthesized samples (araf/xylp = 1/4) were also compression moldable (Fig. 1c). This is the first time that thermal processing has been achieved in AX with such low araf/xylp, i.e., 1/4.

3.3. Thermal properties

DSC analysis was used to determine endothermic transitions. DSC data from AXs (AX_{WB}, AX_{BH}) [Fig. 3a and Figure S10] and AX_{BH} derived thermoplastics (Fig. 3a and 3f–ii, and Figures S12-S15 b and b') show a single glass transition. The presence of dual glass transitions was recorded with DSC for thermoplastics derived from AX_{WB} (Fig. 3a and f (i) and Figures S12-S15 a and a'). These dual transitions are often evident for thermoplastic polymers suggesting phase separation and have been reported for multiblock synthetic polymers (Martello et al., 2014; Zhang et al., 2017), conjugated polymers (Sharma et al., 2019), esterified cellulose (Chen et al., 2018), lignin-based thermoplastics (Saito et al., 2012, 2013), thermoplastic elastomers (TPE) (Gregory et al., 2020) and etherified hemicellulose (Deralia et al., 2021a). The first (lower) glass transition (−75 to −48 °C) likely originated from the extension of the side chain by alkoxide chains in native AX and activated AX [shadowed region annotated as T_g1 in Fig. 3f (i) and (ii)]. The second (upper) glass transition (153–173 °C) can be attributed to thermoplastics derived from the AX_{WB} xylan backbone [shadow region annotated as T_g2 in Fig. 3f (i)]. In contrast, AX_{BH} derived thermoplastics did not show the second glass transition (T_g2) because the glass transition has shifted close to or beyond the degradation temperature (T_d), as is evident in Fig. 3f (ii).

DMA was used to complement the DSC data. Moreover, DMA is more sensitive than DSC for molecular relaxation and thermal transitions because it stresses the sample mechanically while altering its temperature. The thermomechanical response of the compression-molded films of the thermoplastics derived from AX_{WB} and AX_{BH} and the solvent-cast films of AX_{WB} and AX_{BH} was recorded using DMA (Fig. 3g and Figures S16-S20). Note that AX_{WB}, AX_{BH}, A-AX_{WB}, and A-AX_{BH} were solvent-cast because these materials are not compression-molded, and the A-AX films (solvent cast) were too brittle to be measured by DMA. The T_gs obtained from the peaks of the loss modulus are shown in Fig. 3a (blue square) and Table S9. The storage modulus annotated with T_g, loss modulus and tan δ curves are shown in Figures S16-S20. DMA confirmed the presence of the first glass transition in AX_{WB} derived thermoplastics [Fig. 3a, shadowed part in Fig. 3g ii, iii, v, vi (representative DMA curves) and Figures S17-S20].

The alkoxide chains formed after opening the BuGE epoxide ring and specially linked to the hydroxyl groups of the arabinosyl units and ring-opened arabinosyl residues make enough long side chains (Fig. 1b and c) (Deralia et al., 2021a, 2021b, 2021a) to create a separate thermal transition (T_g1 in Fig. 3f–i) corresponding to these side chains. The second glass transition of AX_{WB} derived thermoplastics detected by DSC (T_g2 in Fig. 3f–i) could not be recorded by DMA (Fig. 3g i-iii) because the films became too soft to record the thermal transition above 50 °C.

Note that the differences of 10–20 °C in the T_g values by DSC and DMA (Fig. 3a and Table S8) are likely due to differences in the data collection method (e.g., DMA and DSC measure the dynamic and the thermodynamic signal) (Cao et al., 2020; Saito et al., 2013). The Tg obtained from the E peak is lower than that of the tan δ; however, it has been shown to agree better with the DSC (Cao et al., 2020).

Thermal stability was evaluated using TGA, and Table 2 contains the TGA data. Figure S21 shows the thermograms. The initial degradation (T_{onset}) and inflection ($T_{inflection}$-point of maximum degradation rate) temperatures of thermoplastics derived from AX_{WB} and AX_{BH} (167–223 °C, 227–266 °C) are lower AX and A-AX samples (252–267 °C, 274–286 °C).

The final residue (char content at 500 °C) of A-AX (32–40%) is higher than AX (28–30%). A-AXs after periodate oxidation and reduction reactions may have a large amount of salts, which usually gives a large amount of char yield. AX_{WB} and AX_{BH} derived thermoplastics have lower final residues. In general, these results are consistent with previous reports (Börjesson et al., 2018b, 2019b; Fukuzumi et al., 2009).

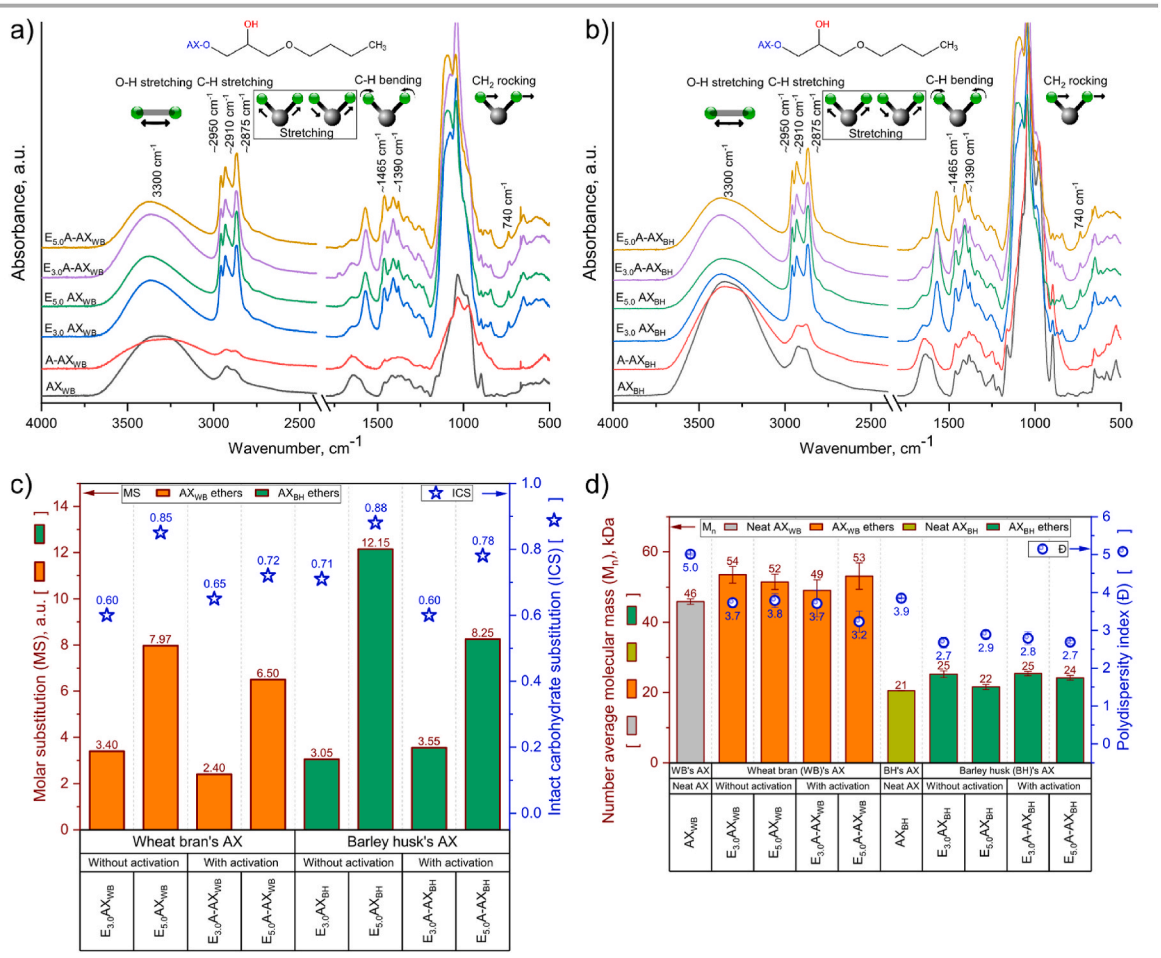

Fig. 2. FTIR spectra of AX, activated AX, AX ether and activated AX ethers derived from **a)** wheat bran arabinoxylan (AX_{WB}), **b)** barley husk arabinoxylan (AX_{BH}), **c)** ^{1}H NMR determined molar substitution (MS) and HPLC determined intact carbohydrate substitution (ICS) of the AX ether and activated AX ether samples, and **d)** Average number molecular masses and polydispersity index of the samples.

3.4. Tensile mechanical properties

The stress-strain behavior of the AX_{WB} and AX_{BH} derived thermoplastics (along with AXs) was determined by uniaxial tensile testing. Representative stress-strain curves are shown in Fig. 4 c-d, and the elastic modulus (E), the tensile strength (σ_t), and the elongation at break (ε_b) are listed in Table 2. All samples show a linear stress-strain relationship with no apparent yield point. As expected, AX_{WB} and AX_{BH} are brittle with a failure strain of 4.3 (±1.1) and 2.4 (±0.7). The mechanical properties of A-AX_{WB} and A-AX_{BH} could not be measured because the films were too brittle to be clamped (Table 2). Decease in molecular weight due to polymer degradation after activation (Börjesson et al., 2018b; Härdelin et al., 2020; Muhammad et al., 2020) can render more brittle films. The AX_{WB} and AX_{BH} derived thermoplastics feature elastomeric behavior, as evident from the higher elongation at break and the low to medium Young's modulus.

Thermoplastics derived from AX_{WB} have greater extensibility (177–301%) compared to thermoplastics derived from AX_{BH} (52–61%) (Table 2). The elongation ranges for AX_{WB} derived thermoplastics are consistent with previously reported values (Börjesson et al., 2019a, 2019b, 2019a). Greater extensibility is achieved at the expense of a reduction in elastic modulus and tensile strength (Ritchie, 2011), as becomes evident from the lower elastic modulus and tensile strength values of thermoplastics derived from AX_{WB} and AX_{BH} compared to AX_{WB} and AX_{BH}. Such high extensibility was never reported for low-araf/xylp AX, i.e., AX_{BH}-derived thermoplastic was processed via compression molding. Solvent-cast films of modified reinforced xylan (with PVA) were shown to have an elongation of up to 133% (Zhang et al., 2018).

The melt processability (Fig. 2b–e) and stretchability (ε_b) of AX_{WB} (Table 2) and (especially AX_{BH} derived thermoplastics (Fig. 4c and d and Table 2) are adequately promising. This encourages us to compare these with polysaccharides (cellulose acetate (Cheng et al., 2006; Fridman and Sorokina, 2006), starch (Huang et al., 2019; Salaberria et al., 2014), xylan (Alekhina et al., 2014; Zhang et al., 2018), arabinoxylan-based (Börjesson et al., 2019a, 2019b, 2019a) and commercial bio-based thermoplastic (polylactic acid-PLA (Martin and Avérous, 2001; Xu and Qu, 2009)) processed using solvent casting and/or industrial polymer processing techniques (Fig. 4e). The best performance, in terms of melt processing and competitive elongation at break, of the AX_{BH} synthesized thermoplastic is evident. This combination of processability and elongation for low araf/xylp arabinoxylan has not been reported in the literature. Similar to our results of AX_{WB} synthesized samples in this work, thermoplastics derived from arabinoxylan (having an araf/xylp ratio between 0.8 and 1.1) with this combination of processability and elongation have been reported in previous reports (Börjesson et al., 2019a, 2019b, 2019a). However, the elongation is better compared to those previously reported. Note that the xylp/araf units have a lower molar ratio than theirs. Araf/Xylp greater than 0.8 might make it more difficult to attach BuGE to side chains because of the presence of arabinosyl units and ring-opened arabinosyl units that have been oxidized and reduced. This might make it more difficult to attach BuGE to side chains.

Cellulose acetate thermoplastics have a poor elongation at break (35

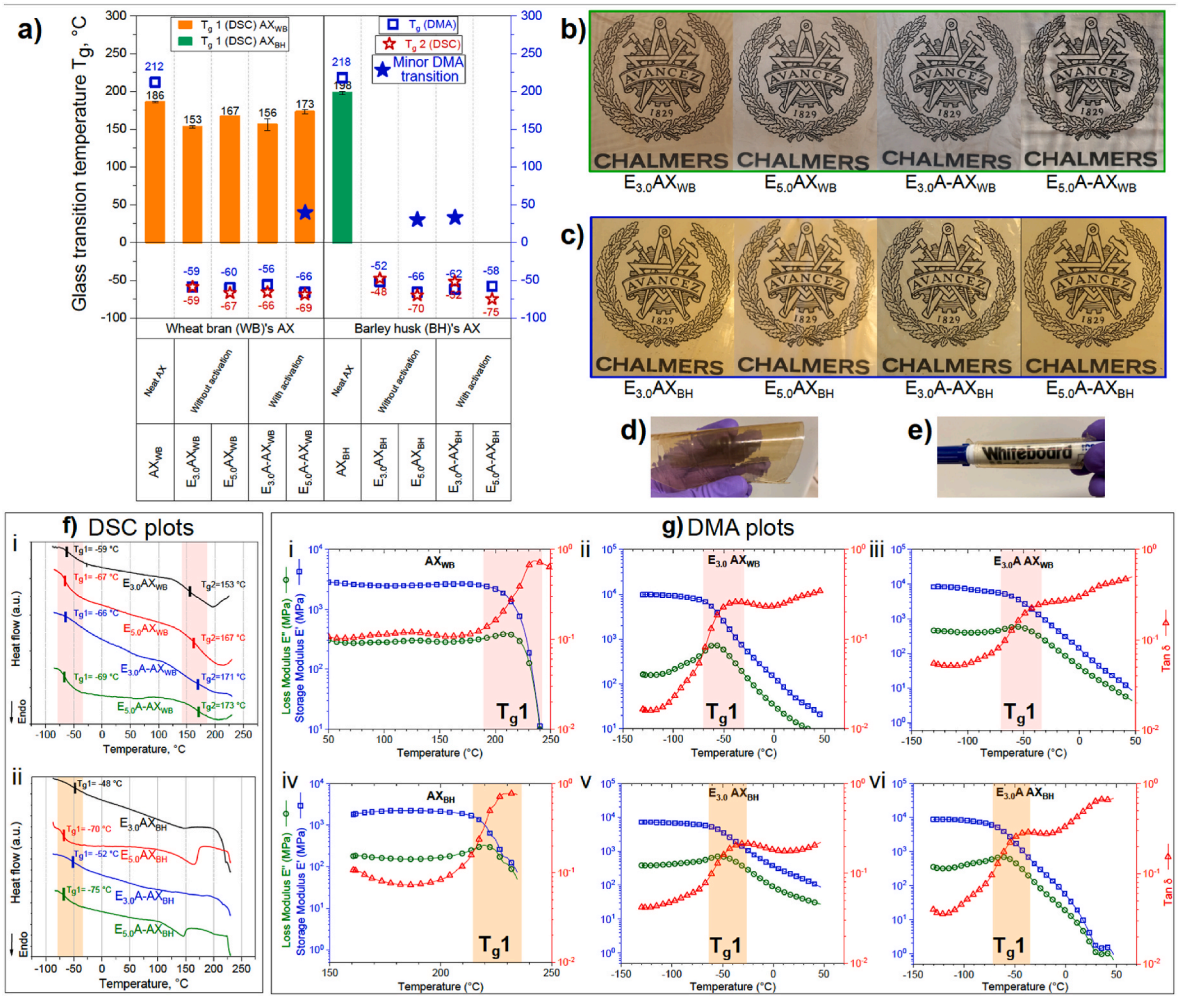

Fig. 3. **a)** DSC and DMA determined T_g of AX, activated AX, AX ether and activated AX samples. T_g1 (orange bar) and T_g2 (green bar) denote the T_g determined from the above-ambient and sub-ambient endotherm transitions of the second heating DSC curves. DMA T_g (blue square) were obtained from the peak of the loss modulus (E) curves. **b)** compression-molded films from AX_{WB} derived samples. **c)** compression-molded films from AX_{BH} derived samples. **d)** example film showing its flexibility. **e)** a representative film folded around a marker to show the foldability of the film. Note: Chalmers logo used with permission and does not claim any copyright. **f)** DSC plots of AX_{WB} and AX_{BH} derived thermoplastics and **g)** Representative DMA curves of AX_{WB} (first row) and AX_{BH} (second row) derived thermoplastics at 3 °C/min, 1 Hz frequency and 0.02% strain. DMA curve of i) AX_{WB}, ii) $E_{3.0}AX_{WB}$, iii) $E_{3.0}A\text{-}AX_{WB}$, iv) AX_{BH}, v) $E_{3.0}AX_{BH}$, vi) $E_{3.0}A\text{-}AX_{BH}$ showing the first glass transition temperature of the two glass transition temperatures. The shadowed part highlights the Tgs from the storage modulus, loss modulus, and Tan δ curves. The second Tg which was >50 °C could not be recorded in DMA as these materials soften above 50 °C. (For interpretation of the references to colour in this figure legend, the reader is referred to the Web version of this article.)

Table 2
Tensile testing and TGA results obtained for AX, activated AX, and thermoplastics derived from AX_{WB} and AX_{BH}.

	Tensile mechanical properties[a]			Thermogravimetric analysis (TGA) data[b]			
Sample ID	E, MPa	σ_t, MPa	ε_b, %	T_{onset}, °C	$T_{inflection}$, °C	T_{endset}, °C	FR, %
AX_{WB}	2672 (153)	70 (11)	4.3 (1.1)	256 (9)	274 (7)	286 (6)	29.6 (1.4)
$A\text{-}AX_{WB}$	–	–	–	267 (5)	286 (2)	307 (4)	40.8 (2.9)
$E_{3.0}AX_{WB}$	7.0 (0.6)	3.0 (0.5)	177 (22)	167 (18)	235 (3)	307 (4)	16.1 (0.2)
$E_{5.0}AX_{WB}$	0.7 (0.1)	0.5 (0.1)	260 (18)	189 (2)	227 (9)	267 (5)	10.7 (0.4)
$E_{3.0}A\text{-}AX_{WB}$	1.4 (0.2)	0.9 (0.3)	270 (49)	223 (1)	292 (1)	317 (1)	18.1 (0.5)
$E_{5.0}A\text{-}AX_{WB}$	0.05 (0.02)	0.03 (0.01)	301 (13)	206 (4)	238 (4)	318 (4)	11.2 (1.0)
AX_{BH}	2455 (395)	40 (6)	2.4 (0.7)	252 (13)	274 (8)	286 (4)	27.9 (1.4)
$A\text{-}AX_{BH}$	–	–	–	263 (1)	282 (0)	296 (1)	32.2 (0.5)
$E_{3.0}AX_{BH}$	40 (2)	4.1 (0.4)	117 (16)	196 (3)	241 (16)	295 (5)	16.3 (1.0)
$E_{5.0}AX_{BH}$	0.9 (0.2)	0.3 (0.06)	52 (6)	206 (4)	251 (1)	275 (1)	13.7 (0.7)
$E_{3.0}A\text{-}AX_{BH}$	3.2 (1.4)	1.2 (0.2)	161 (18)	198 (2)	236 (5)	312 (3)	17.4 (0.7)
$E_{5.0}A\text{-}AX_{BH}$	0.3 (0.09)	0.2 (0.03)	141 (16)	179 (8)	266 (0)	315 (3)	12.1 (0.2)

[a] Data are mean values (n = 5) and the bracketed values are standard deviations; E Young's modulus, σ_t max tensile stress, ε_b tensile strain at break, - data were not available because the solvent cast film was too fragile/brittle.

[b] Data are mean values (n = 2), and the bracketed value is the standard deviation, T_{onset} initial degradation temperature, $T_{inflection}$ temperature at maximum degradation rate, T_{endset} final degradation temperature, final residue (FR)- char content at 500 °C.

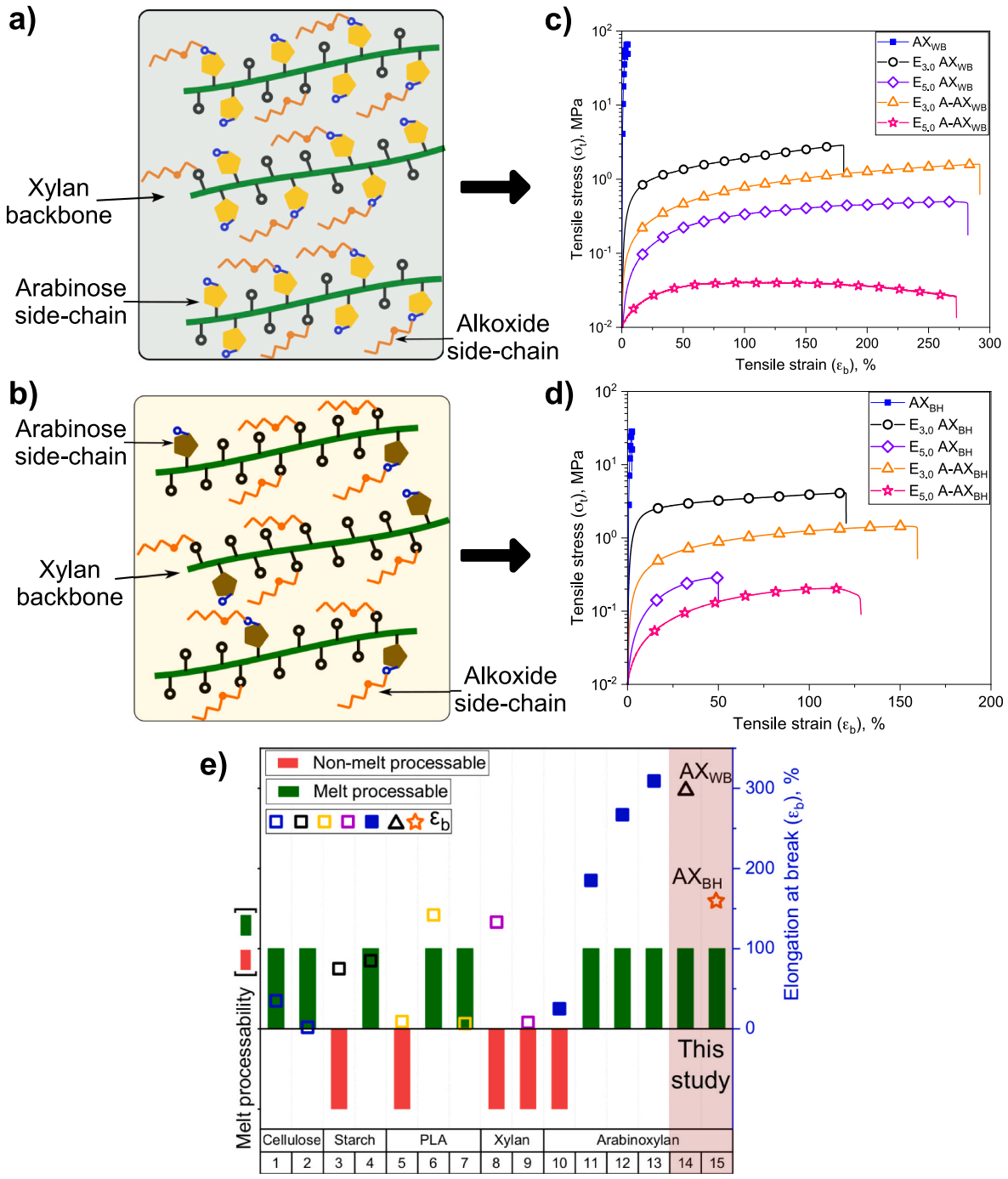

Fig. 4. Proposed thermoplastic structure derived from **a)** AX_{WB} and **b)** AX_{BH}. Representative stress-strain curves of **c)** AX_{WB} and AX_{WB} derived samples, **d)** AX_{BH} and AX_{BH} derived samples. **e)** Melt processability (left y-axis) and elongation at break (right y-axis) of thermoplastics from this study (14 and 15, shadowed part) compared to the literature (1–13, polysaccharide-based and polylactic acid thermoplastics). Figure reference: thermoplastic source (Literature reference) ⇒ 1–2: Cellulose acetate (Cheng et al., 2006; Fridman and Sorokina, 2006), 3–4: starch (Huang et al., 2019; Salaberria et al., 2014), 5–7: polylactic acid-PLA (Martin and Avérous, 2001; Xu and Qu, 2009), 8–9: xylan (Alekhina et al., 2014; Zhang et al., 2018), 10–13: arabinoxylan (Börjesson et al., 2019a, 2019b, 2019a), 14–15: AX_{WB} and AX_{BH} (this work). Table S10 lists the previous literature. Non-melt processable denotes solvent (water or organic) processable. The araf/xylp of AX_{WB} and AX_{BH} are 3/4 and 1/4.

and 2%), but better tensile strength (29 and 26 MPa) compared to the thermoplastics in this study (Cheng et al., 2006; Fridman and Sorokina, 2006). Thermoplastic starch is solvent-processable and meltable, but has lower ε_b than AX_{BH}-derived thermoplastic (Huang et al., 2019; Salaberria et al., 2014). Polylactic acid (PLA) is, although not a commodity plastic, a biobased commercial plastic. It can have similar ε_b with superior tensile strength (Martin and Avérous, 2001; Xu and Qu, 2009). Note that cellulose acetate, starch, and PLA thermoplastic are semicrystalline to highly crystalline structures (Iji et al., 2011). Xylans have never been shown to melt process (Alekhina et al., 2014; Zhang et al., 2018), but they may have comparable ε_b (Zhang et al., 2018).

3.5. *Effect of the structural composition of AX thermoplastics on stretchability*

Both the one-step and two-step strategies enabled thermoplasticity in

the AX_{WB} and AX_{BH} synthesized samples, as shown by compression molding. This suggests that the alkoxide side chains linked to the hydroxyl groups of the xylan backbone and/or intact or ring-opened arabinosyl units in the side chains of AX serve as an effective internal plasticizer. These bonded alkoxide side chains are supposed to reduce the hydrogen bonding between the AX molecules, allowing them to slip over each other when heated above T_g. Such structures were proposed for thermoplastics derived from AX_{WB} and AX_{BH} and are shown in Fig. 4a and b, respectively.

It should be noted that higher alkoxide side chains should attach to the hydroxyl groups of intact or ring-opened arabinosyl units in comparison to the hydroxyl groups of intact or ring-opened xylosyl units in the backbone. This is due to the easy access of the hydroxyl groups of intact or ring-opened arabinosyl units to the side chain. The araf/xylp ratios of AX_{WB} and AX_{BH} are 3/4 and 1/4 (Table S5). Given these facts, the degree of reduction of the hydrogen bonding between AX_{WB} molecules will be higher than that between AX_{BH} molecules. Fig. 4c and d and Table 2 show that the elongation of AX_{WB} derived thermoplastics is greater than that of AX_{BH} derived thermoplastics. These results suggest that the differences in elongation could be explained on the basis of the difference in the araf/xylp.

In this study, a successful attempt to synthesize thermoplastics from the constituent polymers of natural and renewable resources opens up new avenues for the use of agri-waste for value-added materials. Our thermoplastics are partly bioderived because arabinoxylan is biosourced, but *n*-butyl glycidyl ether (BuGE) is currently a petrochemical. The renewable content can surely be increased if BuGE can be obtained from biobased routes or molecules (such as cashew nutshell cardanol or lignin modified to increase its reactivity with arabinoxylan) can be used.

4. Conclusions

In summary, we demonstrate that a one-step and two-step synthesis route could be used to produce flexible and stretchable thermoplastics from low araf/xylp arabinoxylan (AX from barley husk). The synthesis strategy used only direct incorporation of BuGE or pre-activation (successive periodate oxidation and reduction) of AX after incorporation of BuGE. A salient feature of these AXBH-derived thermoplastics is that they could be processed via melt compression molding (one of the industrial polymer processing techniques), which was rare for low-araf/xylp arabinoxylans. This work provides an example of the conversion of a major component of lignocellulose biomass from agricultural waste into a value-added product.

Author contribution

Parveen Kumar Deralia: Conceptualization, Methodology, Data acquisition, Formal analysis, Investigation, Visualization, Writing – original draft, Writing – review & editing. **Amit Kumar Sonker:** Data acquisition, Investigation, Writing – review & editing. **Anja Lund:** Data acquisition, Investigation, Visualization, Writing – review & editing. **Anette Larsson:** Project administration, Funding acquisition, Formal analysis, Visualization, Writing – review & editing. **Anna Ström:** Project administration, Funding acquisition, Formal analysis, Visualization, Writing – review & editing. **Gunnar Westman:** Conceptualization, Methodology, Visualization, Formal analysis, Project administration, Funding acquisition, Supervision, Writing – review & editing.

Declaration of competing interest

The authors declare that they have no known competing financial interests or personal relationships that could have appeared to influence the work reported in this paper.

Acknowledgements

The authors acknowledge Lantmännen for funding research (project number 2017/H017). We are grateful to Hans Theliander and Merima Hasani for granting access to the HPLC and GPC instruments.

Appendix A. Supplementary data

Supplementary data to this article can be found online at https://doi.org/10.1016/j.chemosphere.2022.133618.

References

Alekhina, M., Mikkonen, K.S., Alén, R., Tenkanen, M., Sixta, H., 2014. Carboxymethylation of alkali extracted xylan for preparation of bio-based packaging films. Carbohydr. Polym. 100, 89–96. https://doi.org/10.1016/j.carbpol.2013.03.048.

Amer, H., Nypelö, T., Sulaeva, I., Bacher, M., Henniges, U., Potthast, A., Rosenau, T., 2016. Synthesis and characterization of periodate-oxidized polysaccharides: dialdehyde xylan (DAX). Biomacromolecules 17, 2972–2980. https://doi.org/10.1021/acs.biomac.6b00777.

Apprich, S., Tirpanalan, Ö., Hell, J., Reisinger, M., Böhmdorfer, S., Siebenhandl-Ehn, S., Novalin, S., Kneifel, W., 2014. Wheat bran-based biorefinery 2: valorization of products. LWT - Food Sci. Technol. (Lebensmittel-Wissenschaft -Technol.). https://doi.org/10.1016/j.lwt.2013.12.003.

Averous, L., Pollet, E., 2014. Nanobiocomposites based on plasticized starch. In: Starch Polymers: from Genetic Engineering to Green Applications, pp. 211–239. https://doi.org/10.1016/B978-0-444-53730-0.00028-2.

Börjesson, M., Härdelin, L., Nylander, F., Karlsson, K., Larsson, A., Westman, G., 2018a. Arabinoxylan and nanocellulose from a kilogram-scale extraction of barley husk. Bioresources 13, 6201–6220. https://doi.org/10.15376/biores.13.3.6201-6220.

Börjesson, M., Larsson, A., Westman, G., Ström, A., 2019a. A Process for Preparing Modified Hemicellulose. WO-2019081677-A1.

Börjesson, M., Larsson, A., Westman, G., Ström, A., 2018b. Periodate oxidation of xylan-based hemicelluloses and its effect on their thermal properties. Carbohydr. Polym. 202, 280–287. https://doi.org/10.1016/j.carbpol.2018.08.110.

Börjesson, M., Westman, G., Larsson, A., Ström, A., 2019b. Thermoplastic and flexible films from arabinoxylan. ACS Appl. Polymer Mat. 1, 1443–1450. https://doi.org/10.1021/acsapm.9b00205.

Cao, Z., Galuska, L., Qian, Z., Zhang, S., Huang, L., Prine, N., Li, T., He, Y., Hong, K., Gu, X., 2020. The effect of side-chain branch position on the thermal properties of poly(3-alkylthiophenes). Polym. Chem. 11, 517–526. https://doi.org/10.1039/c9py01026b.

Chen, Z., Zhang, J.J., Xiao, P., Tian, W., Zhang, J.J., 2018. Novel thermoplastic cellulose esters containing bulky moieties and soft segments. ACS Sustain. Chem. Eng. 6, 4931–4939. https://doi.org/10.1021/acssuschemeng.7b04466.

Cheng, G., Wang, T., Zhao, Q., Ma, X., Zhang, L., 2006. Preparation of cellulose acetate butyrate and poly(ethylene glycol) copolymer to blend with poly(3-hydroxybutyrate). J. Appl. Polym. Sci. 100, 1471–1478. https://doi.org/10.1002/app.23135.

Cheng, H.N., Biswas, A., Kim, S., Alves, C.R., Furtado, R.F., 2021. Synthesis and characterization of hydrophobically modified Xylans. Polymers 13, 1–14. https://doi.org/10.3390/polym13020291.

Coates, J., 2006. Interpretation of infrared spectra, A practical approach. In: Encyclopedia of Analytical Chemistry. https://doi.org/10.1002/9780470027318.a5606.

Deralia, P.K., Du Poset, A.M., Lund, A., Larsson, A., Strom, A., Westman, G., 2021a. Oxidation level and glycidyl ether structure determine thermal processability and thermomechanical properties of arabinoxylan-derived thermoplastics. ACS Appl. Bio Mat. 4, 3133–3144. https://doi.org/10.1021/acsabm.0c01550.

Deralia, P.K., du Poset, A.M., Lund, A., Larsson, A., Ström, A., Westman, G., 2021b. Hydrophobization of arabinoxylan with n-butyl glycidyl ether yields stretchable thermoplastic materials. Int. J. Biol. Macromol. 188, 491–500. https://doi.org/10.1016/j.ijbiomac.2021.08.041.

Farhat, W., Venditti, R., Ayoub, A., Prochazka, F., Fernández-de-Alba, C., Mignard, N., Taha, M., Becquart, F., 2018. Towards thermoplastic hemicellulose: chemistry and characteristics of poly-(ε-caprolactone) grafting onto hemicellulose backbones. Mater. Des. 153, 298–307. https://doi.org/10.1016/j.matdes.2018.05.013.

Fredon, E., Granet, R., Zerrouki, R., Krausz, P., Saulnier, L., Thibault, J.F., Rosier, J., Petit, C., 2002. Hydrophobic films from maize bran hemicelluloses. Carbohydr. Polym. 49, 1–12. https://doi.org/10.1016/S0144-8617(01)00312-5.

Fridman, O.A., Sorokina, A.V., 2006. Criteria of efficiency of cellulose acetate plasticization. Polym. Sci. B 48, 233–236. https://doi.org/10.1134/S1560090406090028.

Fukuzumi, H., Saito, T., Iwata, T., Kumamoto, Y., Isogai, A., 2009. Transparent and high gas barrier films of cellulose nanofibers prepared by TEMPO-mediated oxidation. Biomacromolecules 10, 162–165. https://doi.org/10.1021/bm801065u.

Gebruers, K., Dornez, E., Boros, D., Fraś, A., Dynkowska, W., Bedo, Z., Rakszegi, M., Delcour, J.A., Courtin, C.M., 2008. Variation in the content of dietary fiber and components thereof in wheats in the healthgrain diversity screen. J. Agric. Food Chem. 56, 9740–9749. https://doi.org/10.1021/jf800975w.

Gregory, G.L., Sulley, G.S., Carrodeguas, L.P., Chen, T.T.D., Santmarti, A., Terrill, N.J., Lee, K.Y., Williams, C.K., 2020. Triblock polyester thermoplastic elastomers with semi-aromatic polymer end blocks by ring-opening copolymerization. Chem. Sci. 11, 6567–6581. https://doi.org/10.1039/d0sc00463d.

Hansen, N.M.L., Plackett, D., 2008. Sustainable films and coatings from hemicelluloses: a review. Biomacromolecules. https://doi.org/10.1021/bm800053z.

Härdelin, L., Bernin, D., Börjesson, M., Ström, A., Larsson, A., 2020. Altered thermal and mechanical properties of spruce galactoglucomannan films modified with an etherification reaction. Biomacromolecules 21, 1832–1840. https://doi.org/10.1021/acs.biomac.9b01730.

Hartman, J., Albertsson, A.C., Sjöberg, J., 2006. Surface- and bulk-modified galatoglucomannan hemicellulose films and film laminates for versatile oxygen barriers. Biomacromolecules 7, 1983–1989. https://doi.org/10.1021/bm060129m.

Huang, L., Xu, H., Zhao, H., Xu, M., Qi, M., Yi, T., An, S., Zhang, X., Li, C., Huang, C., Wang, S., Liu, Y., 2019. Properties of thermoplastic starch films reinforced with modified cellulose nanocrystals obtained from cassava residues. New J. Chem. 43, 14883–14891. https://doi.org/10.1039/c9nj02623a.

Ibn Yaich, A., Edlund, U., Albertsson, A.C., 2017. Transfer of biomatrix/wood cell interactions to hemicellulose-based materials to control water interaction. Chem. Rev. https://doi.org/10.1021/acs.chemrev.6b00841.

Iji, M., Moon, S., Tanaka, S., 2011. Hydrophobic, mechanical and thermal characteristics of thermoplastic cellulose diacetate bonded with cardanol from cashew nutshell. Polym. J. 43, 738–741. https://doi.org/10.1038/pj.2011.57.

Izydorczyk, M.S., Dexter, J.E., 2008. Barley β-glucans and arabinoxylans: molecular structure, physicochemical properties, and uses in food products-a Review. Food Res. Int. https://doi.org/10.1016/j.foodres.2008.04.001.

Jain, R.K., Sjöstedt, M., Glasser, W.G., 2000. Thermoplastic xylan derivatives with propylene oxide. Cellulose. https://doi.org/10.1023/A:1009260415771.

Köhnke, T., Pujolras, C., Roubroeks, J.P., Gatenholm, P., 2008. The effect of barley husk arabinoxylan adsorption on the properties of cellulose fibres. Cellulose 15, 537–546. https://doi.org/10.1007/s10570-008-9209-5.

Laine, C., Harlin, A., Hartman, J., Hyvärinen, S., Kammiovirta, K., Krogerus, B., Pajari, H., Rautkoski, H., Setälä, H., Sievänen, J., Uotila, J., Vähä-Nissi, M., 2013. Hydroxyalkylated xylans - their synthesis and application in coatings for packaging and paper. Ind. Crop. Prod. 44, 692–704. https://doi.org/10.1016/j.indcrop.2012.08.033.

Martello, M.T., Schneiderman, D.K., Hillmyer, M.A., 2014. Synthesis and melt processing of sustainable poly(ε-decalactone)-block-poly(lactide) multiblock thermoplastic elastomers. ACS Sustain. Chem. Eng. 2, 2519–2526. https://doi.org/10.1021/sc500412a.

Martin, O., Avérous, L., 2001. Poly(lactic acid): plasticization and properties of biodegradable multiphase systems. Polymer 42, 6209–6219. https://doi.org/10.1016/S0032-3861(01)00086-6.

Mathew, A.P., Dufresne, A., 2002. Morphological investigation of nanocomposites from sorbitol plasticized starch and tunicin whiskers. Biomacromolecules. https://doi.org/10.1021/bm0101769.

Mikkonen, K.S., Laine, C., Kontro, I., Talja, R.A., Serimaa, R., Tenkanen, M., 2015. Combination of internal and external plasticization of hydroxypropylated birch xylan tailors the properties of sustainable barrier films. Eur. Polym. J. 66, 307–318. https://doi.org/10.1016/j.eurpolymj.2015.02.034.

Muhammad, M., Willems, C., Rodríguez-Fernández, J., Gallego-Ferrer, G., Groth, T., 2020. Synthesis and characterization of oxidized polysaccharides for in situ forming hydrogels. Biomolecules 10, 1185. https://doi.org/10.3390/biom10081185.

Nypelö, T., Laine, C., Aoki, M., Tammelin, T., Henniges, U., 2016. Etherification of wood-based hemicelluloses for interfacial activity. Biomacromolecules 17, 1894–1901. https://doi.org/10.1021/acs.biomac.6b00355.

Peresin, M.S., Kammiovirta, K., Setälä, H., Tammelin, T., 2012. Structural features and water interactions of etherified xylan thin films. J. Polym. Environ. 20, 895–904. https://doi.org/10.1007/s10924-012-0469-7.

Pitkänen, L., Virkki, L., Tenkanen, M., Tuomainen, P., 2009. Comprehensive multidetector HPSEC study on solution properties of cereal arabinoxylans in aqueous and DMSO solutions. Biomacromolecules 10, 1962–1969. https://doi.org/10.1021/bm9003767.

Ritchie, R.O., 2011. The conflicts between strength and toughness. Nat. Mater. https://doi.org/10.1038/nmat3115.

Ruthes, A.C., Martínez-Abad, A., Tan, H.T., Bulone, V., Vilaplana, F., 2017. Sequential fractionation of feruloylated hemicelluloses and oligosaccharides from wheat bran using subcritical water and xylanolytic enzymes. Green Chem. 19, 1919–1931. https://doi.org/10.1039/c6gc03473j.

Saito, T., Brown, R.H., Hunt, M.A., Pickel, D.L., Pickel, J.M., Messman, J.M., Baker, F.S., Keller, M., Naskar, A.K., 2012. Turning renewable resources into value-added polymer: development of lignin-based thermoplastic. Green Chem. 14, 3295–3303. https://doi.org/10.1039/c2gc35933b.

Saito, T., Perkins, J.H., Jackson, D.C., Trammel, N.E., Hunt, M.A., Naskar, A.K., 2013. Development of lignin-based polyurethane thermoplastics. RSC Adv. 3, 21832–21840. https://doi.org/10.1039/c3ra44794d.

Salaberria, A.M., Labidi, J., Fernandes, S.C.M., 2014. Chitin nanocrystals and nanofibers as nano-sized fillers into thermoplastic starch-based biocomposites processed by melt-mixing. Chem. Eng. J. 256, 356–364. https://doi.org/10.1016/j.cej.2014.07.009.

Schooneveld-Bergmans, M.E.F., Beldman, G., Voragen, A.G.J., 1999. Structural features of (glucurono)arabinoxylans extracted from wheat bran by barium hydroxide. J. Cereal. Sci. 29, 63–75. https://doi.org/10.1006/jcrs.1998.0222.

Selig, M.J., Thygesen, L.G., Felby, C., Master, E.R., 2015. Debranching of soluble wheat arabinoxylan dramatically enhances recalcitrant binding to cellulose. Biotechnol. Lett. 37, 633–641. https://doi.org/10.1007/s10529-014-1705-0.

Sharma, A., Pan, X., Bjuggren, J.M., Gedefaw, D., Xu, X., Kroon, R., Wang, E., Campbell, J.A., Lewis, D.A., Andersson, M.R., 2019. Probing the relationship between molecular structures, thermal transitions, and morphology in polymer semiconductors using a woven glass-mesh-based DMTA technique. Chem. Mater. 31, 6740–6749. https://doi.org/10.1021/acs.chemmater.9b01213.

Sheldon, R.A., Brady, D., 2018. The limits to biocatalysis: pushing the envelope. Chem. Commun. 54, 6088–6104. https://doi.org/10.1039/c8cc02463d.

Siller, M., Amer, H., Bacher, M., Roggenstein, W., Rosenau, T., Potthast, A., 2015. Effects of periodate oxidation on cellulose polymorphs. Cellulose 22, 2245–2261. https://doi.org/10.1007/s10570-015-0648-5.

Sluiter, A., Hames, B., Ruiz, R., Scarlata, C., Sluiter, J., Templeton, D., 2010–2011. Determination of Structural Carbohydrates and Lignin in Biomass Determination of Structural Carbohydrates and Lignin in Biomass. National Renewable Energy Laboratory (NREL) https://doi.org/NREL/TP-510-42618.

Stepan, A.M., Höije, A., Schols, H.A., De Waard, P., Gatenholm, P., 2012. Arabinose content of arabinoxylans contributes to flexibility of acetylated arabinoxylan films. J. Appl. Polym. Sci. 125, 2348–2355. https://doi.org/10.1002/app.36458.

Svärd, A., Brännvall, E., Edlund, U., 2018. Modified and thermoplastic rapeseed straw xylan: a renewable additive in PCL biocomposites. Ind. Crop. Prod. 119, 73–82. https://doi.org/10.1016/j.indcrop.2018.03.067.

Wang, J., Somasundaran, P., 2006. Mechanisms of ethyl(hydroxyethyl) cellulose-solid interaction: influence of hydrophobic modification. J. Colloid Interface Sci. https://doi.org/10.1016/j.jcis.2005.06.072.

Xu, Y.Q., Qu, J.P., 2009. Mechanical and rheological properties of epoxidized soybean oil plasticized poly(lactic acid). J. Appl. Polym. Sci. 112, 3185–3191. https://doi.org/10.1002/app.29797.

Zepnik, S., Kabasci, S., Kopitzky, R., Radusch, H.J., Wodke, T., 2013. Extensional flow properties of externally plasticized cellulose acetate: influence of plasticizer content. Polymers 5, 873–889. https://doi.org/10.3390/polym5030873.

Zhang, J., Deubler, R., Hartlieb, M., Martin, L., Tanaka, J., Patyukova, E., Topham, P.D., Schacher, F.H., Perrier, S., 2017. Evolution of microphase separation with variations of segments of sequence-controlled multiblock copolymers. Macromolecules 50, 7380–7387. https://doi.org/10.1021/acs.macromol.7b01831.

Zhang, X., Liu, C., Zhang, A., Sun, R., 2018. Synergistic effects of graft polymerization and polymer blending on the flexibility of xylan-based films. Carbohydr. Polym. 181, 1128–1135. https://doi.org/10.1016/j.carbpol.2017.11.025.